Advanced Powder Technology 29 (2018) 349–358

Contents lists available at ScienceDirect

Advanced Powder Technology

journal homepage: www.elsevier.com/locate/apt

Original Research Paper

Effect of Magnetized Ethanol on the Shape Evolution of Zinc Oxide from Nanoparticles to Microrods: Experimental and Molecular Dynamic Simulation Study

Hamed Rashidi [a,*], Ali Ahmadpour [b], Mostafa Gholizadeh [c], Fatemeh F. Bamoharram [d], Fatemeh Moosavi [c]

[a] Department of Chemical Engineering, Shahrood Branch, Islamic Azad University, P.O. Box 36155-163, Shahrood, Iran
[b] Department of Chemical Engineering, Ferdowsi University of Mashhad, Mashhad, Iran
[c] Department of Chemistry, Faculty of Science, Ferdowsi University of Mashhad, Mashhad, 91775-1436, Iran
[d] Research Centre for Animal Development Applied Biology – Department of Nanobiotechnology, Mashhad Branch, Islamic Azad University, Mashhad, Iran

ARTICLE INFO

Article history:
Received 7 May 2017
Received in revised form 6 November 2017
Accepted 15 November 2017
Available online 24 November 2017

Keywords:
Zinc oxide
Solvothermal
Magnetic field
Electron microscopy
Molecular dynamics simulation

ABSTRACT

In the current research, ethanol was exposed to an external magnetic field, called magnetized ethanol, and then, used as a solvent in the solvothermal method to synthesize various ZnO structures. Moreover, the morphologies of the synthesized structures are compared with those obtained using ordinary ethanol. The attained results evidently demonstrated the formation of ZnO nanoparticles and microrods by using ordinary and magnetized ethanol, respectively. Moreover, X-ray diffraction (XRD) and scanning electron microscopy (SEM) were utilized for characterizing the synthesized ZnO structures. The XRD results demonstrated that the synthesized products are in Zincite hexagonal phase. Besides, molecular dynamics simulation suggested that the molecular mobility is diminished upon using the magnetic field. It was found that the interactions among ZnO particles were enhanced by the slight increase in the magnetic field while the number of interactions between ZnO and solvent was reduced revealing the magnetic-field-induced particle growth from the molecular level insight.

1. Introduction

Since the properties of final products depend on the particles' shape and size, the main objective in the synthesis of different materials is to control these two parameters. Due to the relatively high exciton binding energy (60 meV) and a wide direct band gap (3.37 eV), and also, its various shape-induced functions, zinc oxide has gained a great deal of attention. ZnO structures with various shapes and sizes have different applications ranging from catalysis for photo-catalytic degradation to solar cell preparation, gas sensors [1–8] and antibacterial properties [9].

In recent years, both fundamental and applied researches have been concentrated on the morphologically controllable synthesis of ZnO because of its unique electrical, acoustic and optical properties [10–13]. Various methods, such as mechanochemical, sol-gel, direct precipitation, azeotropic distillation, freeze drying, ethanol washing, chemical vapor deposition and hydrothermal processing have been used in the preparation of ZnO structures [9,14–27]. Because of their advantages such as low cost, simple routes and low-temperature processes, the hydrothermal and solvothermal techniques have been widely used for the synthesis of nanostructured materials like ZnO crystals [28–30].

In the solvothermal technique, the solvent plays a vital role in the properties of synthesized crystals. Besides, solubility and transport behavior of the precursors can be strongly affected by the properties of a solvent such as polarity and viscosity. Therefore, various crystalline compounds in different shapes and sizes could be produced by only changing the type of solvent [10–12,30–32]. The choice of proper solvent for crystallization might impose profound effects on the morphology of synthesized particles. Investigation on the solvent magnetization revealed that some unique properties could be generated in the solvent subsequently leading to the synthesis of altered structures.

In the recent years, the magnetic field has been used for enhancement of heat transfer coefficient in heat transfer applications like heat pipes which contain magnetic particles [33–36], while studies on the effect of magnetic field on solvent's properties are relatively rare. The effect of magnetic field on properties of water has been discovered in the early 1900s by Danish Physicist

* Corresponding author.
E-mail address: hrashidi@iau-shahrood.ac.ir (H. Rashidi).

https://doi.org/10.1016/j.apt.2017.11.022

Hendricks Anton Lorenz [37]. In that research, protic solvents, i.e. water and ethanol, were exposed to a magnetic field. His observation demonstrated that by passing water through a magnetic field, the electron pattern in the ions was changed [38]. It is also reported that if water is exposed to an external magnetic field, different phenomena would occur. Magnetization of the solvent influenced the hydrogen bond distribution resulting in an increase in the water viscosity and enthalpy as well as a decrease in the surface tension [39–42].

The influence of magnetic field on macroscopic features and microscopic structures of water has been previously studied by Xiao-Feng and Bo [43]. They have detected some variations in the water properties once exposed to the magnetic field. They have also measured the changes in surface tension, contact angle, viscosity, rheology, refractive index, dielectric constant and electrical conductivity of the magnetized water by using infrared, Raman, visible light, ultraviolet and X-ray techniques. It has been shown that although the distribution of molecules and transition probability of valence, bonded and inner-layer electrons were varied, the constitution of molecules and atoms remained unchanged. In addition, the magnetic field has been found to be responsible for the reduction of the contact angle, surface tension force, and hydrophobicity of water while the refractive index, dielectric constant and electric conductivity of water were increased. The viscosity of magnetized water could be enhanced by increasing the intensity of magnetic field and magnetized time. Likewise, the effect of magnetic treatment on the surface tension reduction of water was investigated by Amiri and Dadkhah [42]. They have reported a reduction in the surface tension of pure water with increasing the number of times water passes through the magnetic field. An 8% reduction in the surface tension of magnetically treated water is reported elsewhere [44]. Rohani and Entezari have investigated the synthesis of manganese oxide nanocrystals in the presence of magnetic field. They have demonstrated that larger and smaller sizes of nanoparticles could be obtained with and without magnetic treatment, respectively [45]. In addition, the external magnetic field retards the nucleation process which accelerates the crystal growth leading to an increased amount of rod-like structure.

We have recently investigated some applications of magnetization in various processes [38,39,46–49]. To the best of our knowledge, among all magnetized solvents, the role and behavior of magnetized ethanol have been vastly overlooked, and no capability has been mentioned for this popular solvent. As a result, there is a great interest to delineate the effect of magnetized ethanol on material synthesis. In continuation of our previous works on the synthesis of various ZnO structures as well as applications of magnetized solvents [38,39,47,50–54], and also due to the importance of ZnO structures in nanotechnology, photocatalysis, and several other industries, the major aim of the current work is to investigate the influence of induced magnetic field applied to ethanol on the morphology of zinc oxide prepared by the solvothermal technique.

For a deeper understanding of the processes, classical molecular dynamics (MD) simulations is also performed to determine the extent of enhanced hydrogen-bonding and local environmental structures [55–57], indicating that MD simulation is a powerful tool to decipher the local features at the molecular level. In addition, MD helps the researchers to understand different properties including macroscopic and microscopic ones. However, the formation of rod structures in a specific solvent has not been investigated by MD simulation so far. Assessment of the magnetization process from the molecular viewpoint was also performed to explore the size and configuration of particles in ethanol illustrating the effect of the aspect ratio and the particle-particle interactions on the aggregate structures of ZnO rod-like particles.

2. Materials and methods

2.1. Solvent magnetizing apparatus

A permanent magnet in a compact form was used. This equipment was a coaxial static magnetic system (AQUA CORRECT, H.P. S Co., Germany) with the field strength of 0.6 T. The two ends of this equipment were connected to the liquid pump and the solvent reservoir. Solutions could flow through a coaxial static magnet and return to the solvent reservoir. Therefore, the solution might pass throughout the magnetic field several times in a closed cycle (Fig. 1).

2.2. Synthesis method

Zinc acetate dehydrate and ethanol (both analytical grades) have been purchased from Merck Company. Zinc acetate dehydrate (0.02 mmol) was dissolved in ethanol (ordinary/magnetized) (30–40 mL) under vigorous stirring. Ethanol was magnetized at various times (1 pass, 10 min, and 120 min) in the case of magnetized ethanol. After mixing for about 10 min, the reaction mixture was transferred into the Teflon-lined stainless steel autoclave (50 mL), which was maintained at 130 °C for 48 h followed by cooling naturally to the room temperature. To remove all impurities, the white precipitates were separated by centrifuge, washed several times with deionised water and ethanol and then dried at 60 °C for 8 h to get a white fine powder. This powder was used for further characterizations.

2.3. Measurements and analysis

The crystal structure of Zinc oxide samples was characterized by X-ray diffraction (XRD, Bruker D8 Advance) using Cu-Kα radiation (λ = 1.5406 Å). The surface morphology of powders was studied using scanning electron microscope (SEM, LEO 1450 VP, Zeiess, Germany). Furthermore, the energy dispersive X-ray spectroscopy (EDS, 7353, Axford, England) was used for the elemental analysis. FTIR spectroscopy, within the wave number range of 850 and 4000 cm^{-1}, was employed with a Bruker 500 scientific spectrometer. The conductivity of solvent was determined using an Accumet AR20.

2.4. Simulation details

By employing a hybrid density functional theory incorporating Becke's three-parameter exchange with Lee, Yang and Parr's (B3LYP) correlation functional [58,59], density functional theory (DFT) calculation for ethanol system was performed using

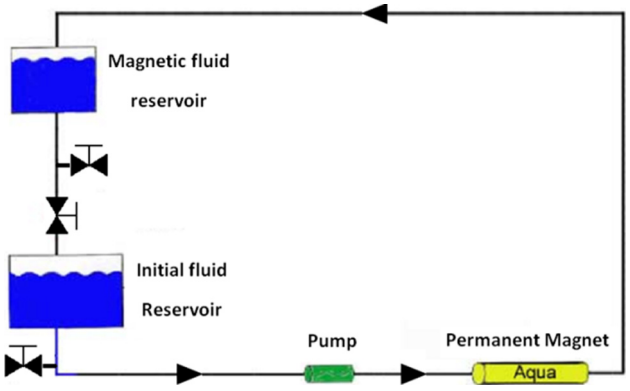

Fig. 1. The schematic of solvent magnetization apparatus.

Gaussian 03 program [60]. The geometry of the lowest-energy conformer was optimized at B3LYP/6-311++G(d,p) level of theory by applying the default criteria for convergence of the ab initio calculations. The molecular electrostatic potential (ESP) was computed to shed light on the effective localization of electron-rich regions in the molecular system [61]. Vibrational analysis demonstrated that the optimized structure is at the local minimum; consequently, geometrical parameters including bond lengths, bond angles and dihedral angles computed at B3LYP/6-311++G(d,p) level of theory as well as atomic charges were implemented in order to construct the initial configuration. Atomic charges were calculated from CHelpG method [62]. It is worthy to mention that the natural bond orbital (NBO) analysis was also performed to compute atomic charges [63,64]. The results of simulations confirmed that the earlier values for atomic charges lead to more accurate density which is in excellent agreement with the experimental values at ambient conditions (298.15 K and 1 bar) with insignificant deviation error of 0.98% [65] as well as calculated density [66] and simulation values [67]. In addition, different force fields including OPLS [68], AMBER [69] and DREIDING [70] were applied to explore the role of the force field on the accuracy of the results. In this way, the force field applied is validated. The results notably showed that OPLS potential model conducts simulation to the most accurate results which are in good agreement with the previous MD and MC simulations [67,71]. As a result, all simulations for the pure solvent were performed based on OPLS force field by the help of ESP results for long-range electrostatic interactions. Long-range electrostatic interactions were accounted by using Ewald procedure [72–76] within the isothermal-isobaric (*NPT*) ensemble at 298.15 K. 1 ns simulation was performed to achieve accurate density at the pressure of 1.0 bar. The ensemble of simulation was NPT and cut-off distance of 16 Å was considered to truncate the long-range potential energy. The coupling methods for pressure and temperature were applied by Nose-hoover thermostat-barostat [77] every 1.0 and 0.1 ps, respectively. Verlet leapfrog scheme [76] was applied to compute the positions and velocities of particles with time step 1 fs. After reaching the equilibrium state, the system keeps running for 300 ps to achieve the input for the next step of the simulation. In order to collect the required data with the applied potential model, the last configuration was applied for another simulation with *NVT* (constant number of particles, constant volume, and constant temperature) ensemble. All the conditions were kept the same as previous simulation.

The external constant magnetic field perpendicular to the z-direction was applied to the pure solvent and its mixture with ZnO particles. All MD simulations were conducted using the software DL_POLY version 2.17 [78].

In the present study, we pursued the potential "storing" of energy from exposures to a 6.5 T static magnetic field. It is assumed that the changes in the solvent diffusion altered viscosity which was explained from the molecular aspect. An accurate practical means for the analysis of the structure is provided by the radial distribution function, RDF, of the pair atoms which is defined as the local number density, ρ(r), at the radius r divided by the system number density, ρ_0:

$$g(r) = \frac{\rho(r)}{\rho_0} = \frac{V \cdot dN(r, \Delta r)}{N \cdot 4\pi r^2 dr} \quad (1)$$

in which N is the number of molecules, V is system volume, and $dN(r, \Delta r)$ is the number of molecules within the shell volume of r at the radius r.

In MD, the mean squared displacement (MSD) is an indication of the diffusion phenomenon. It is defined according to

$$MSD = \langle |r_j(t) - r_j(0)| \rangle^2 \quad (2)$$

in which r_j(t) and r_j(0) denote the position vectors of atom j at time t and 0, respectively. The growth rate of MSD depends on the number of times that an atom suffers collisions per unit time.

3. Results and discussion

3.1. Experimental part

Preparation of ZnO structures employed in this work was carried out by the solvothermal method using ordinary and magnetized ethanol. Solvothermal synthesis typically involves the preparation of solid materials from reagents dissolved in an aqueous solution under mild temperature and pressure. In this study, various ZnO structures are synthesized by the reaction of $Zn(CH_3COO)_2{\cdot}2H_2O$ with ethanol. The chemical reactions can be expressed as [79]:

$$CH_3COO^- + HOCH_2CH_3 \rightarrow OH^- + CH_3COOCH_2CH_3 \quad (3)$$

$$Zn^{2+} + 2OH^- \rightarrow ZnO \downarrow + H_2O \quad (4)$$

OH^- is gradually released based on the first reaction, and then, according to the second reaction, Zn^{2+} cations react with OH^- anions to form ZnO structure under solvothermal conditions. In other words, the weak esterification reaction (Eq. (3)) liberates OH^- and then ZnO clusters are momentarily formed (Eq. (4)). Hexagonal ZnO crystal has a positively polar zinc face and a negatively polar oxygen face [79]. Therefore, in order to minimize the total surface energy, ZnO clusters tend to aggregate and self-assemble into the metastable structures.

Fig. 2 shows typical X-ray diffraction (XRD) patterns of the as-prepared ZnO structures using ordinary ethanol. The appeared peaks in Fig. 2 correspond to reflections from 100, 002, 101, 102, 110, 103 and 112 crystal planes which identify the hexagonal Zincite crystalline type. There are no diffraction peaks can be observed from other impurities which indicates that the pure ZnO structure has been produced.

In order to investigate the effect of using magnetized ethanol on the crystallinity of the synthesized ZnO particles, XRD pattern of a sample, produced with magnetized ethanol, was also recorded (Fig. 3).

From Fig. 3, the sharp peaks correspond to the reflections from 100, 002, 101, 102, 110, 103, 200, 112, 201, 004 and 202 crystal planes, respectively, which can be attributed to the hexagonal Zincite crystalline structure of ZnO. Thus, it can be concluded that upon using the magnetized ethanol, ZnO structures with excellent crystallinity can be produced. Moreover, there could be detected

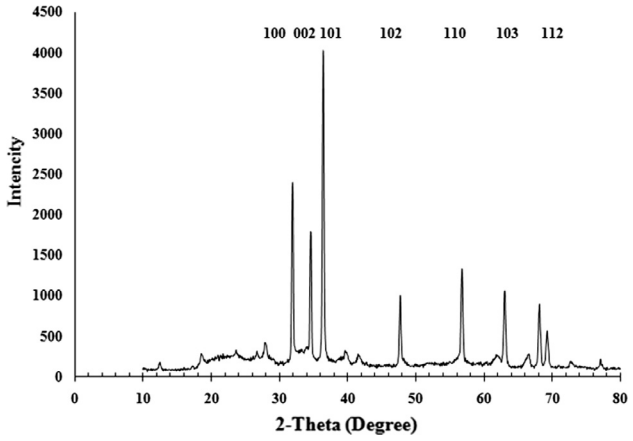

Fig. 2. XRD pattern of the synthesized ZnO structure using ordinary ethanol.

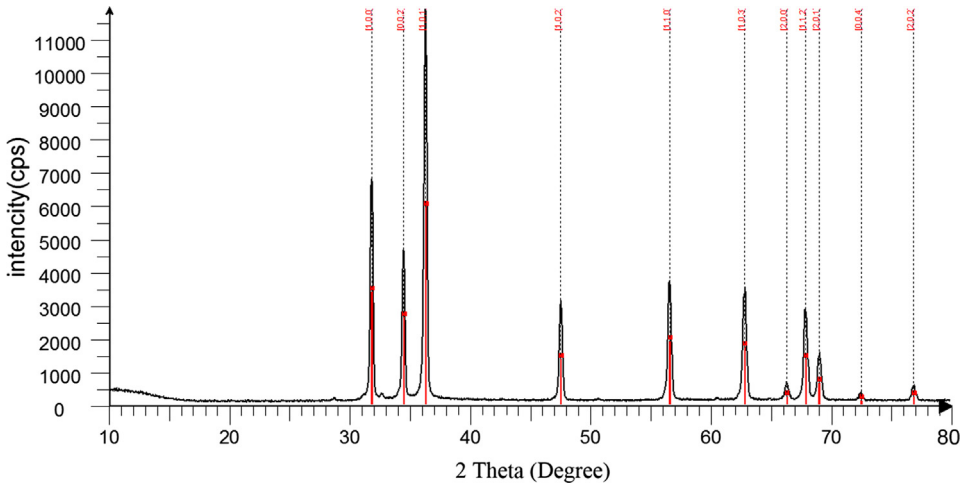

Fig. 3. XRD pattern of the synthesized ZnO structure using the magnetized ethanol.

no additional peaks in the XRD pattern (Fig. 3) indicating the formation of extra pure ZnO structures using magnetized ethanol. Comparing Figs. 2 and 3, it can be inferred that upon the use of magnetized ethanol, the diffraction peaks of ZnO structure have become sharper implying the larger size of the as-formed crystals.

3.1.1. Ordinary ethanol

At first, ZnO structures were prepared in the presence of ordinary ethanol. SEM results shown in Fig. 4a and b indicate that ZnO nanoparticles are produced with ordinary ethanol. According to those images, the average size of ZnO nanoparticles is about 100 nm and they are completely recognizable from each other.

3.1.2. Magnetized ethanol

In another series of experiments, ZnO structures were produced using the magnetized ethanol. Fig. 4c and d shows SEM images of the sample prepared in the presence of one-pass magnetized ethanol. Remarkably, upon the use of the magnetized ethanol, the morphology of sample became utterly different. As a result, it can be clearly concluded that the properties of ethanol have been changed by applying the magnetic field. It is necessary to mention that this phenomenon is different from the Zeeman's effect which is highly diminished in the absence of magnetic field while the memory of magnetic treatment remains over 200 h [80].

With respect to Fig. 4c and d, it is clear that ZnO particles with hexagonal structure are produced. Based on these experiments, it is suggested that magnetization of solvent results in the formation of a suitable amount of ZnO cluster nuclei for their subsequent growth. It has been reported that magnetic treatment could enhance the rates of nucleation and crystal growth [81]. In addition, the magnetized ethanol enhances the activity of ZnO nuclei which are assembled into hexagonal structures. A similar

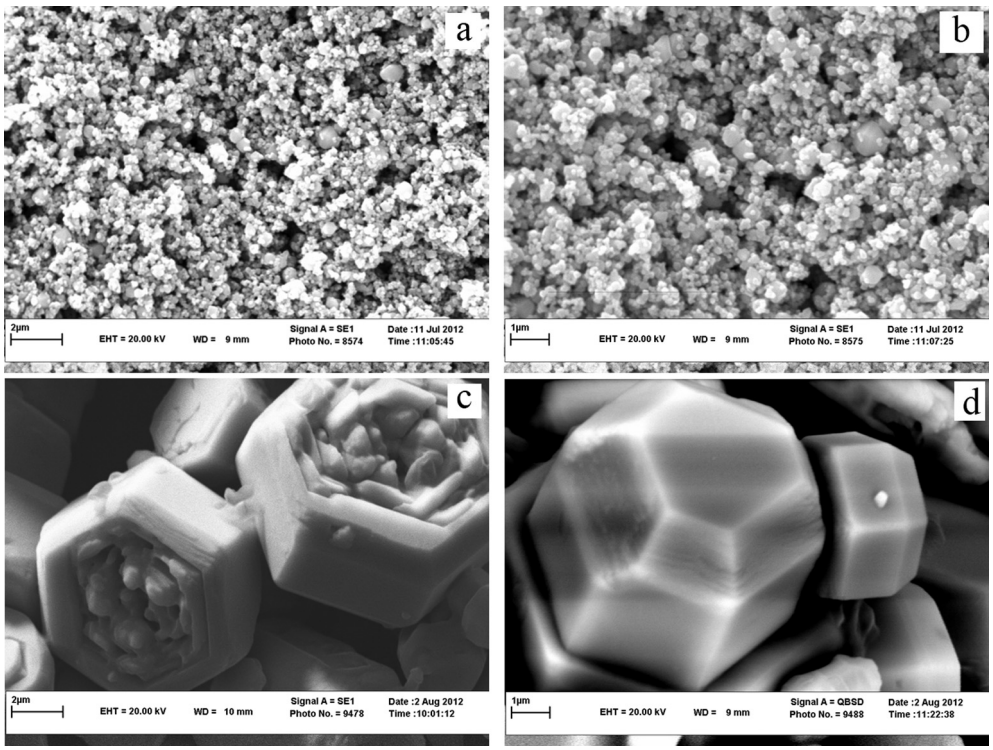

Fig. 4. SEM images of ZnO nanoparticles prepared in the presence of; (a, b) ordinary ethanol and (c, d) magnetized ethanol (one pass magnetization).

mechanism has been observed in another study once the ultrasonic pre-treatment was employed [82]. It is suggested that the subsequent inner rings are formed inside the first hexagonal structure, and then, the crystal growth continues layer by layer to form the structures shown in Fig. 4c and d. The crystal formation process can be divided into two main stages, namely, nucleation and crystal growth. The size and morphology of the given crystals are greatly affected by some external conditions such as magnetization through participating in nucleation and growth stages. As a result, the process was influenced by several factors [83].

The general operating principle for the magnetic technology is a result of physics behind the interactions between a magnetic field and a moving electric charge. A magnetic force is exerted on each ion as soon as the ions are placed in the magnetic field. According to Fig. 5, the forces on ions of opposite charges are exerted in the opposite directions. Fig. 5 demonstrates the influential factors on the force of magnetic field. The magnetic field force or Lorenz force can be obtained by using Eq. (5):

$$F = |A||B|Q\sin\theta \tag{5}$$

where F is the magnetic field force, A is the lines of magnetic field, B is the fluid current, Q is the number of charged particles dissolved in the fluid, and θ is the angle between magnetic field and fluid direction which is always vertical. Therefore, according to Eq. (4), the maximum magnetic force is obtained when θ is equal to 90° and hence, Eq. (4) can be simplified as [39]:

$$F = |A||B|Q \tag{6}$$

Since ethanol is a polar protic solvent like water, a similar behavior for both of them would be expected when they are exposed to the magnetic field. The molecular arrangement of water is changed as exposed to the magnetic field. The surface tension of water also reduces to a certain value after a few treatment cycles [41], and its activity is improved due to the reduction of cluster sizes leading to a change in the molecular energy. In addition, it has been shown that the number of hydrogen bonds in the liquid structure and the self-diffusion coefficient of molecules are influenced by the magnetic field [84]. It can be concluded that the competition between different hydrogen bond networks leads to a weakened intra-cluster hydrogen bonding, and consequently, the smaller clusters are formed with stronger inter-cluster hydrogen bonds. Other researchers have demonstrated that the number of hydrogen bonds increases by approximately 0.34% when the magnetic field strength increased from 1 T to 10 T [84]. A rather similar effect may be expected once ethanol is exposed to the magnetic field. As a proof of the occurred changes in the hydrogen bonds, the FTIR spectra of magnetized ethanol at different times are presented in Fig. 6.

The peaks observed at 1055 and 2980 cm^{-1} can be attributed to C—O and C—H stretching vibration bonds, respectively, which are the characteristic bonds of ethanol. Besides, the appeared peak at about 3350 cm^{-1} is ascribed to O—H stretching vibration. As seen in Fig. 6, the peak at about 3350 cm^{-1} is broadened and its intensity is reduced indicating that the number of hydrogen bonds increases with enhancing the magnetization time. The conductivity values of ordinary and magnetized ethanol were also measured and shown in Fig. 7.

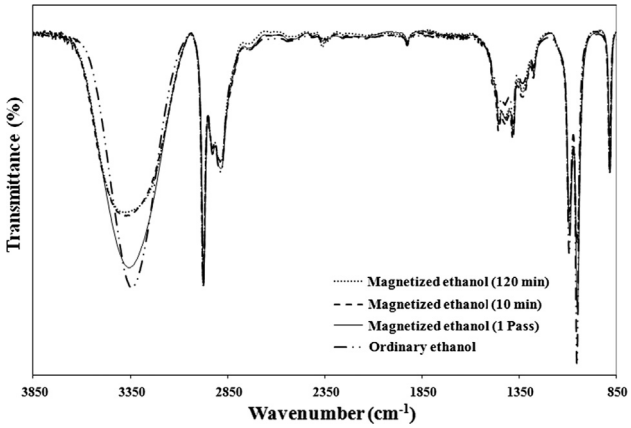

Fig. 6. FTIR spectra of ordinary and magnetized ethanol with different magnetization times.

Based on Fig. 7, the conductivity of ethanol rises as the magnetization time increases. A similar observation was reported when water is exposed to an external magnetic field [43]. This phenomenon is due to the enhancement of charged particles, e.g. OH^- in the presence of magnetized ethanol, however, according to the various interpretations, the basic mechanism for the magnetic treatment effects is not well understood yet.

A remarkable change was observed in the morphology of prepared samples. In order to shed some light on the challenge and investigate the effect of solvent magnetization time, additional experiments were performed with different magnetization times. Fig. 8a and b shows SEM images of the sample prepared via a 10 min magnetization of ethanol. Based on this figure, it is clearly seen that the ZnO microrods are synthesized. The prepared microrods have hexagonal structures based on Fig. 8a and b. These results imply that the growth mechanism is changed due to the longer magnetization time (10 min) of the solvent. Such interesting behavior can be explained by the fact that, at the beginning, a suitable amount of ZnO nuclei is formed and later on, the ZnO nuclei are self-adjusted into hexagonal plates before growing into rods. Afterwards, the growth continues layer by layer to form the ZnO microrods. A similar mechanism has also been reported elsewhere

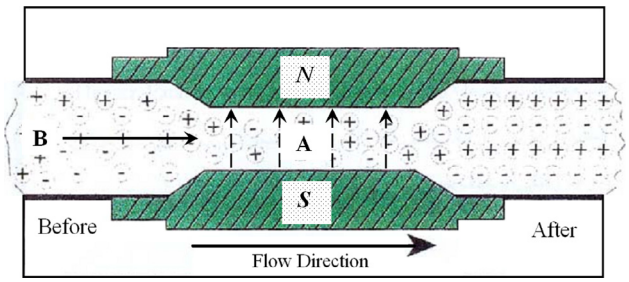

Fig. 5. Schematic diagram of magnetization process.

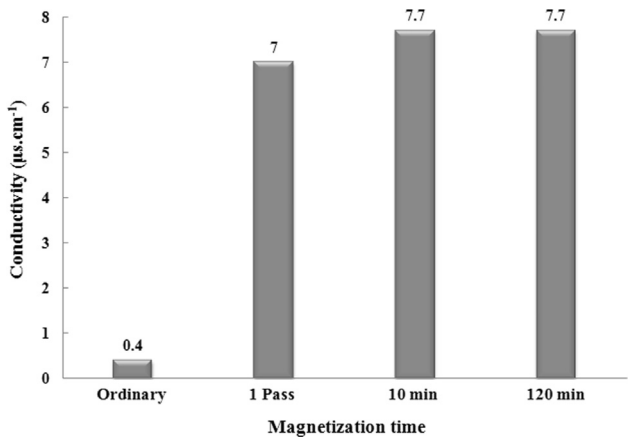

Fig. 7. Conductivity of ordinary and magnetized ethanol.

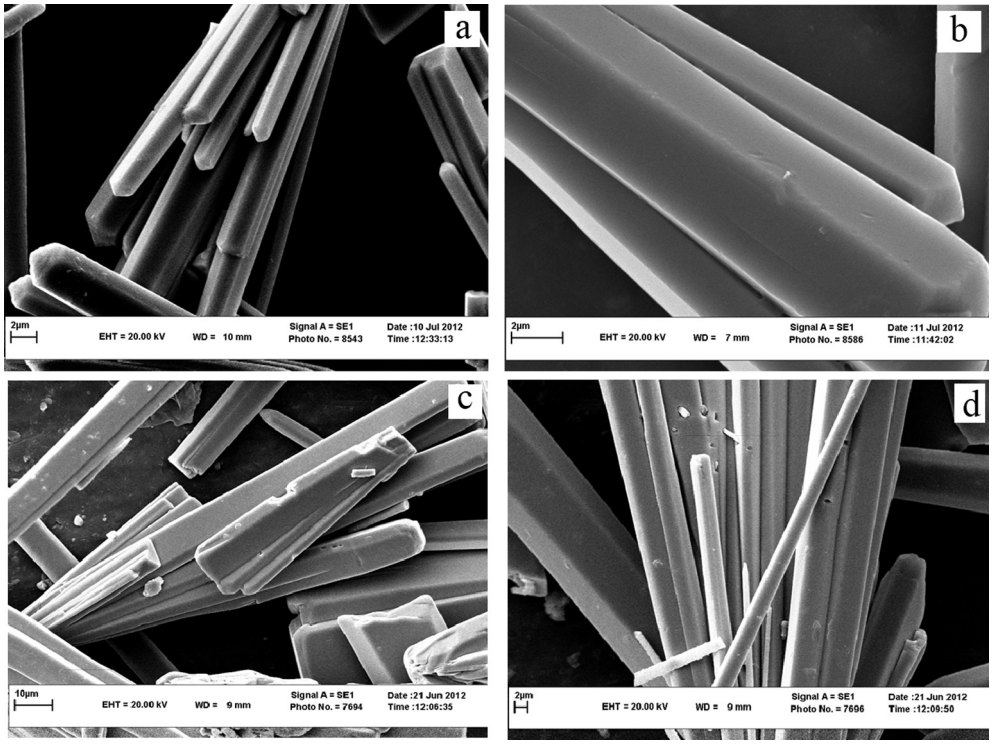

Fig. 8. SEM images of ZnO microrods prepared in the presence of; (a, b) magnetized ethanol (10 min magnetization) and (c, d) magnetized ethanol (120 min magnetization).

[82]. Based on Fig. 8a and b, the prepared ZnO microrods exhibit a nearly uniform size distribution with an average diameter of around 2 μm. It has been reported that the external magnetic field could promote one-dimensional growth in the crystals as a result of which, the rod-like structures are formed [45,80,85,86].

By increasing the magnetization time of ethanol up to 120 min, the morphology of the prepared sample shows an insignificant change and the only difference is the increased microrods' diameter (Fig. 8c and d).

Thus, according to the employed experimental details, one could infer that the solvent plays a key role in the morphology of the synthesized ZnO structures in the solvothermal method. It is indicated that the solvent magnetization can change the formation mechanism of ZnO crystals and also the orientation of crystal growth.

3.2. Molecular dynamics part

As expected, the formation of hydrogen bonding between the ethanol solvent molecules might be enhanced upon the use of an external magnetic field, which is one of the considerable issues in the present research. Fig. 9 compares the variation in number of hydrogen bonds in terms of simulation time in ethanol in the presence and absence of a magnetic field.

As can be seen, the structure of the treated solvent is directly affected by applying a magnetic field; but based on a different viewpoint, the molecules are more ordered and stable, and their interaction force is stronger than that of the untreated solvent. Structurally, it can be found by exploring $g_{O\cdots H}(r)$ of the system. As Fig. 10 illustrates, for the current system, the distance between two solvent molecules decreases from 1.825 Å to 1.775 Å by applying the magnetic field. To evaluate the average number of hydrogen bonds, the present study adopts the geometric criterion [87], that is, a hydrogen bond would be formed if the distance between the oxygen and hydrogen atoms of a pair-molecule is less than the first minimum of the O···H radial distribution function, 2.625 Å in

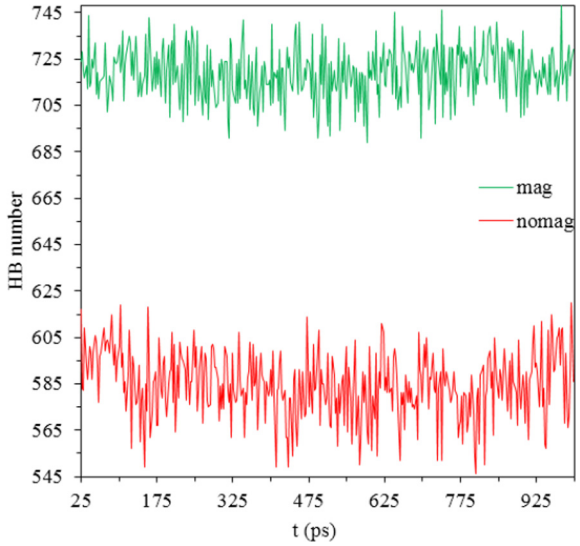

Fig. 9. The variation of hydrogen bonding number with simulation time in the presence and absence of magnetic field.

the case of untreated solvent and 2.425 Å in the case of treated one. The procedure has been applied to water molecules by Levitt et al. [88]. The simulation results presented in Fig. 10 indicate that employing of a magnetic field intensifies the strength of hydrogen bonding. The slight decrease in the O···H distances with magnetic field enhances the networking ability. Moreover, the smaller distance between H and O atoms of the ethanol molecules implies that the cluster size has been increased under the magnetic field, and hence, a more closely packed structure of ethanol molecules is observed.

The results demonstrate that the number of hydrogen bonds between the ethanol molecules increases in accordance with the

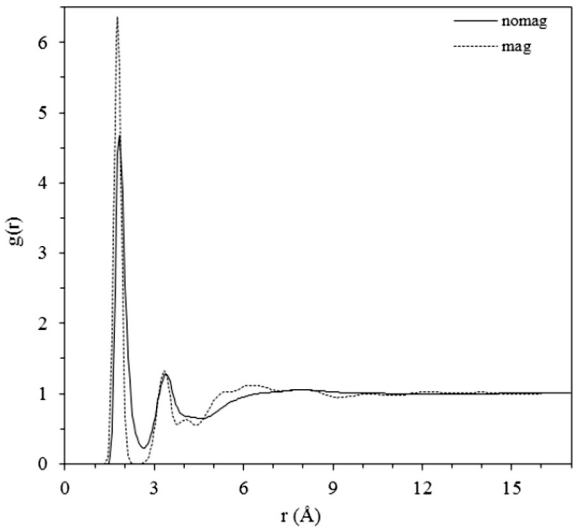

Fig. 10. Comparison of g(r) O···H in the presence and absence of the magnetic field.

results reported in the case of water by Hosoda et al. [56]. It has been suggested that electron delocalization of the hydrogen-bonded molecules enhances hydrogen-bond strength under an external magnetic field.

The results of simulation illustrated that the distance between two ethanol molecules in the absence and presence of the magnetic field is decreased by a value of 5.00 pm. In other words, the slight compactness of ethanol molecules was observed because of the magnetic field.

The mobility of the solvent may also be affected by the magnetic field. Noticeably, applying the magnetic field to the pure solvent leads to a lower value of self-diffusion coefficient for the molecules implying a lower level of solvent fluidity.

Since the aim of the current work is to evaluate the effect of an external magnetic field on the synthesis of ZnO nanoparticles, MD simulation results revealed that the size distribution depends on the external magnetic field. It is proposed that interactions of the magnetic field with particles present in the system may cause the growth of nanoparticles to be improved; and consequently, the exerted forces on ZnO particles before and after magnetization was computed. Quite interestingly, it was found that the attraction force on the particles, due to the magnetic field, is stronger than the non-magnetized condition. In other words, an external magnetic field has a significant effect on the morphology of the particles and could decrease the distances between particles. In addition, a snapshot of the last configuration of the system after 4 ns of simulation in the presence of magnetic field is compared with the ordinary system further confirming the abovementioned standpoint (see Fig. 11).

As the figure illustrates, the impact of an external magnetic field on the morphology of the particles as well as the size distribution is in accordance with the experimental results. In other words, the solution consists of elongated ZnO particles.

However, to gain a deeper insight into the behaviour of the system at external magnetic field, RDF of the oxygen atom of ZnO particles and the hydrogen atom of the solvent were studied. The interactions between these two atoms, i.e., O(Zn)···H(O) interactions, are quite strong. The mentioned distance, based on RDF, decreases from 2.375 Å to 2.275 Å by applying the magnetic field demonstrating the strength of the interactions between ZnO particles and ethanol solvent. Fig. 12 illustrates more details in spite of the lower number of solvents around particles that may be a witness of a more close-distance between ZnO particles due to the magnetic field. For confirmation of this result, Fig. 13 compares the variation of hydrogen bond numbers versus configuration

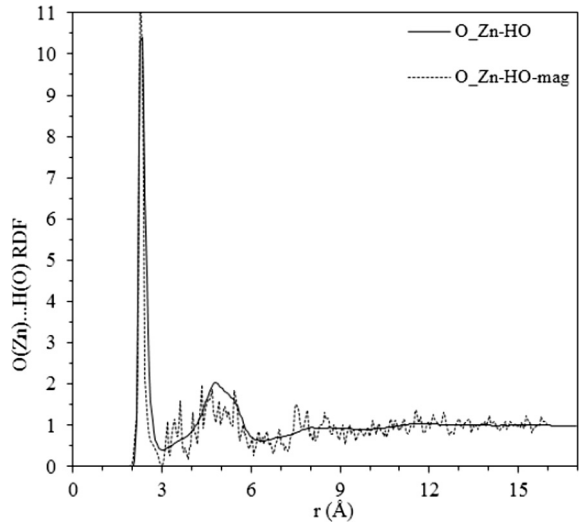

Fig. 12. Pair correlation function between ZnO particles and solvent in the presence and absence of the magnetic field.

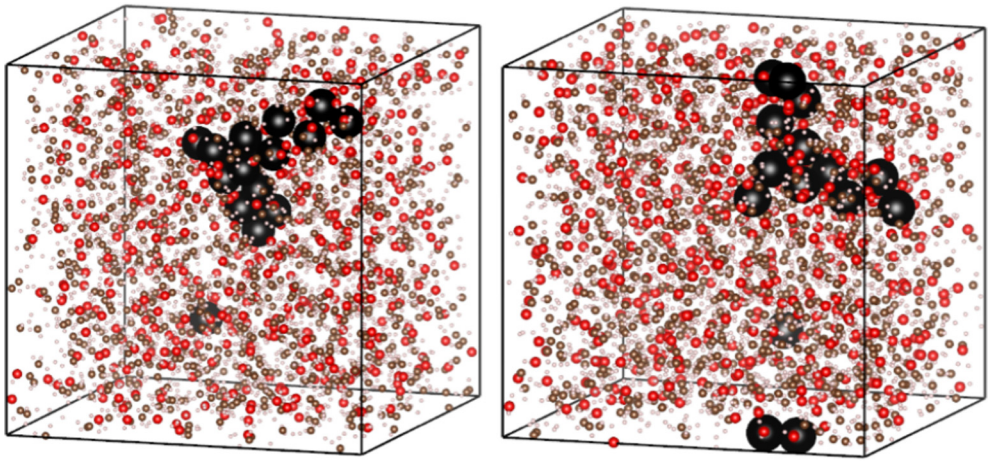

Fig. 11. A snapshot of the last configuration of the system after 4 ns simulation in the presence (right side) and absence (left side) of the magnetic field.

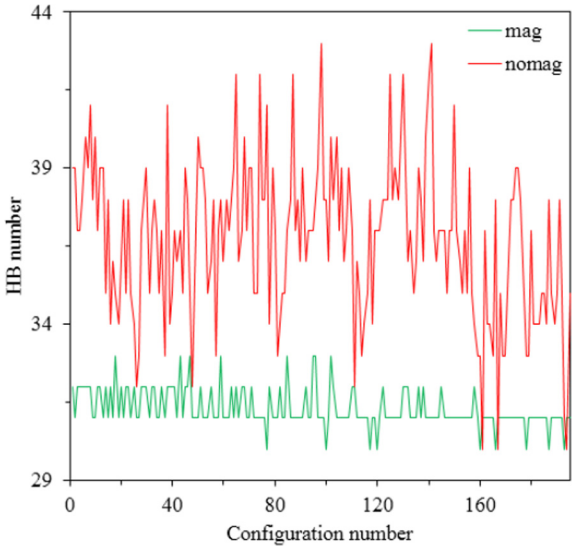

Fig. 13. Number of interactions between the particles and solvent for magnetized system and non-magnetized one.

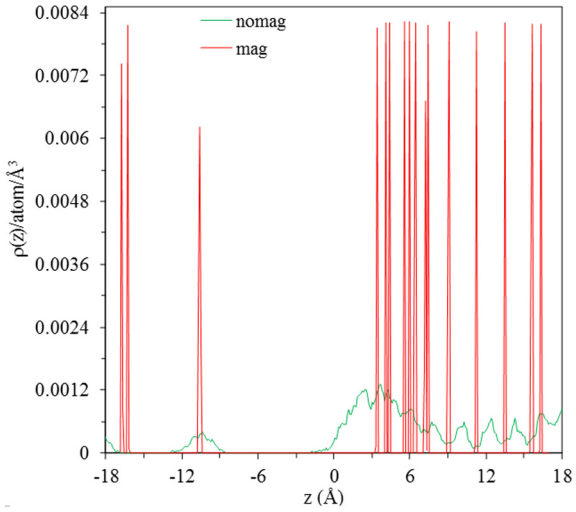

Fig. 14. Number density of nanoparticle along z direction in the magnetized system and non-magnetized one.

number of simulation due to the magnetic field. The progressive reduction in the number of hydrogen bonds between the particles and solvent upon application of a magnetic field further explicates the stronger interactions of the particles and their larger size.

Taking into account the density profile of the nanoparticle will all reveal that applying magnetic field has changed the distribution and size of the ZnO particles in the solvent. Fig. 14 shows the variation of z-density of ZnO particles along the z direction.

On the base of atomic density at z direction, it can be understood that the density enjoys a considerable increase in the magnetized solvent that is a sign of aggregation of nanoparticle. Another approve for this idea is the Zn···Zn distance that decreases if magnetic field is applied. Fig. 15 shows the time revolution of ZnO distance during the simulation.

As the figure illustrates, at the presence of magnetic field Zn···Zn distance is constant about 3.39 Å while this distance observes a significant fluctuation between 3.19 Å and 3.78 Å in the untreated solvent. In other words, the aggregation of nanoparticle is improved in treated solvent. Typically, based on the above findings, it seems that the structure of the ethanol solvent

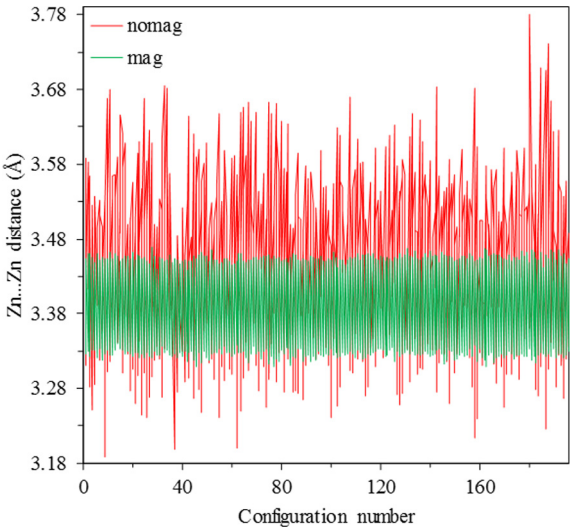

Fig. 15. The comparison of Zn···Zn distance with time of simulation between magnetized and non-magnetized system.

undergoes some changes upon exposing to the magnetic field which probably affects the ZnO particle size.

4. Conclusions

In this study, various ZnO structures were prepared in the presence of magnetized and ordinary ethanol by using the solvothermal technique. The attained results demonstrated that magnetization of ethanol has a remarkable impact on the morphology of the synthesized ZnO particles which can be controlled by varying the time periods of solvent magnetizations. By using ordinary ethanol, only ZnO nanoparticles were produced while ZnO microrods were synthesized as a result of using the magnetized ethanol. It can be concluded that the magnetized ethanol accelerates the crystal growth and increases the amounts of rod-like structures. In addition, molecular dynamics simulation was applied to examine the effect of a static magnetic field on the ZnO particle size and morphology at ambient conditions. It was shown that an external magnetic field would have a direct effect on the number of hydrogen bonds, their strength and the structure of ethanol as well as its molecular mobility. Enhancing the number of hydrogen bonds in a pure solvent as a result of an external magnetic field, causes the formation of larger ethanol molecular clusters. Furthermore, the magnetic field induces a tighter bonding between solvent's molecules.

Molecular mobility was reduced upon application of an external magnetic field; on the other hand, the magnetic field constrains the movement of the solvent molecules which is in good agreement with the decreased movement of ZnO particles in spite of their tendency to maintain a smaller distance from each other and produce larger particles. Atom-atom pair correlation functions as well as density profile, made available from the histogram of trajectories, were used to estimate the spreading profile, and thus, the structural relation between particles. Quite importantly, the resulting particles are relatively stable and the stronger force on ZnO particles as well as the weaker interactions between the solvent and the particles could be detected after the magnetization process.

Compliance with ethical standards

Conflict of interest

The authors declare that they have no conflict of interest.

Acknowledgments

This work is financially supported by Ferdowsi University of Mashhad – Iran (no. 3/15902).

References

[1] G.M. Hamminga, G. Mul, J.A. Moulijn, Real-time in situ ATR-FTIR analysis of the liquid phase hydrogenation of -butyrolactone over Cu-ZnO catalysts: a mechanistic study by varying lactone ring size, Chem. Eng. Sci. 59 (2004) 5479–5485.
[2] C. Feldmann, Polyol-mediated synthesis of nanoscale functional materials, Adv. Funct. Mater. 13 (2003) 101–107.
[3] M.J. Zheng, L.D. Zhang, G.H. Li, W.Z. Shen, Fabrication and optical properties of large-scale uniform zinc oxide nanowire arrays by one-step electrochemical deposition technique, Chem. Phys. Lett. 363 (2002) 123–128.
[4] J. Xu, Q. Pan, Y.A. Shun, Z. Tian, Grain size control and gas sensing properties of ZnO gas sensor, Sens. Actuators, B 66 (2000) 277–279.
[5] Z.S. Wang, C.H. Huang, Y.Y. Huang, Y.J. Hou, P.H. Xie, B.W. Zhang, H.M. Cheng, A highly efficient solar cell made from a dye-modified ZnO-covered TiO_2 nanoporous electrode, Chem. Mater. 13 (2001) 678–682.
[6] R. Hong, Z. Ren, J. Ding, H. Li, Experimental investigation and particle dynamic simulation for synthesizing titania nanoparticles using diffusion flame, Chem. Eng. J. 108 (2005) 203–212.
[7] R. Hong, T. Pan, J. Qian, H. Li, Synthesis and surface modification of ZnO nanoparticles, Chem. Eng. J. 119 (2006) 71–81.
[8] R. Turton, D.A. Berry, T.H. Gardner, A. Miltz, Evaluation of zinc oxide sorbents in a pilot-scale transport reactor: sulfidation kinetics and reactor modeling, Ind. Eng. Chem. Res. 43 (2004) 1235–1243.
[9] D.H. Piva, R.H. Piva, M.C. Rocha, J.A. Dias, O.R.K. Montedo, I. Malavazi, M.R. Morelli, Antibacterial and photocatalytic activity of ZnO nanoparticles from Zn $(OH)_2$ dehydrated by azeotropic distillation, freeze drying, and ethanol washing, Adv. Powder Technol. 28 (2017) 463–472.
[10] K.G. Kanade, B.B. Kale, R.C. Aiyer, B.K. Das, Effect of solvents on the synthesis of nano-size zinc oxide and its properties, Mater. Res. Bull. 41 (2006) 590–600.
[11] M. Wang, S.H. Hahn, J.S. Kim, J.S. Chung, E.J. Kim, K.-K. Koo, Solvent-controlled crystallization of zinc oxide nano(micro)disks, J. Cryst. Growth 310 (2008) 1213–1219.
[12] J. Ma, C. Jiang, Y. Xiong, G. Xu, Solvent-induced growth of ZnO microcrystals, Powder Technol. 167 (2006) 49–53.
[13] C. Ma, B. Zhao, Q. Dai, B. Fan, G. Shao, R. Zhang, Porous structure to improve microwave absorption properties of lamellar ZnO, Adv. Powder Technol. 28 (2017) 438–442.
[14] T. Tsuzuki, P.G. McCormick, ZnO nanoparticles synthesized by mechanochemical processing, Scr. Mater. 44 (2001) 1731–1735.
[15] K. Okuyama, I. Wuled Lenggoro, Preparation of nanoparticles via spray route, Chem. Eng. Sci. 58 (2003) 537–547.
[16] F. Rataboul, C. Nayral, M.J. Casanove, A. Maisonnat, B. Chaudret, Synthesis and characterization of monodisperse zinc and zinc oxide nanoparticles from the organometallic precursor $[Zn(C_6H_{11})_2]$, J. Organomet. Chem. 643–644 (2002) 307–312.
[17] Y.W. Koh, M. Lin, C.K. Tan, Y.L. Foo, K.P. Loh, Self-assembly and selected area growth of zinc oxide nanorods on any surface promoted by an aluminum precoat, J. Phys. Chem. B 108 (2004) 11419–11425.
[18] W. Yu, X. Li, X. Gao, Catalytic synthesis and structural characteristics of high-quality tetrapod-like ZnO nanocrystals by a modified vapor transport process, Cryst. Growth Des. 5 (2004) 151–155.
[19] X.L. Hu, Y.J. Zhu, S.W. Wang, Sonochemical and microwave-assisted synthesis of linked single-crystalline ZnO rods, Mater. Chem. Phys. 88 (2004) 421–426.
[20] J. Wang, L. Gao, Synthesis and characterization of ZnO nanoparticles assembled in one-dimensional order, Inorg. Chem. Commun. 6 (2003) 877–881.
[21] J.H. Kim, W.C. Choi, H.Y. Kim, Y. Kang, Y.-K. Park, Preparation of mono-dispersed mixed metal oxide micro hollow spheres by homogeneous precipitation in a micro precipitator, Powder Technol. 153 (2005) 166–175.
[22] H. Zhang, D. Yang, Y. Ji, X. Ma, J. Xu, D. Que, Low temperature synthesis of flowerlike ZnO nanostructures by cetyltrimethylammonium bromide-assisted hydrothermal process, J. Phys. Chem. B 108 (2004) 3955–3958.
[23] B. Liu, H.C. Zeng, Hydrothermal synthesis of ZnO nanorods in the diameter regime of 50 nm, J. Am. Chem. Soc. 125 (2003) 4430–4431.
[24] M. Singhai, V. Chhabra, P. Kang, D.O. Shah, Synthesis of ZnO nanoparticles for varistor application using Zn-substituted aerosol ot microemulsion, Mater. Res. Bull. 32 (1997) 239–247.
[25] M.S. Tokumoto, S.H. Pulcinelli, C.V. Santilli, V. Briois, Catalysis and temperature dependence on the formation of ZnO nanoparticles and of zinc acetate derivatives prepared by the sol–gel route, J. Phys. Chem. B 107 (2003) 568–574.
[26] R. Viswanathan, G.D. Lilly, W.F. Gale, R.B. Gupta, Formation of zinc oxide–titanium dioxide composite nanoparticles in supercritical water, Ind. Eng. Chem. Res. 42 (2003) 5535–5540.
[27] G. Escalante, H. Juárez, P. Fernández, Characterization and sensing properties of ZnO film prepared by single source chemical vapor deposition, Adv. Powder Technol. 28 (2017) 23–29.
[28] K. Byrappa, T. Adschiri, Hydrothermal technology for nanotechnology, Prog. Cryst. Growth Charact. Mater. 53 (2007) 117–166.
[29] H.Y. Xu, H. Wang, Y.C. Zhang, W.L. He, M.K. Zhu, B. Wang, H. Yan, Hydrothermal synthesis of zinc oxide powders with controllable morphology, Ceram. Int. 30 (2004) 93–97.
[30] S.H. Yu, Hydrothermal/solvothermal processing of advanced ceramic materials, J. Ceram. Soc. Jpn. 109 (2001) 65–75.
[31] J.S. Lee, S.C. Choi, Solvent effect on synthesis of indium tin oxide nano-powders by a solvothermal process, J. Eur. Ceram. Soc. 25 (2005) 3307–3314.
[32] J.H. ter Horst, R.M. Geertman, G.M. van Rosmalen, The effect of solvent on crystal morphology, J. Cryst. Growth 230 (2001) 277–284.
[33] M. Afrand, N. Sina, H. Teimouri, A. Mazaheri, M.R. Safaei, M.H. Esfe, J. Kamali, D. Toghraie, Effect of magnetic field on free convection in inclined cylindrical annulus containing molten potassium, Int. J. Appl. Mech. 07 (2015) 1550052.
[34] H.R. Goshayeshi, M. Goodarzi, M. Dahari, Effect of magnetic field on the heat transfer rate of kerosene/Fe_2O_3 nanofluid in a copper oscillating heat pipe, Exp. Therm. Fluid Sci. 68 (2015) 663–668.
[35] H.R. Goshayeshi, M. Goodarzi, M.R. Safaei, M. Dahari, Experimental study on the effect of inclination angle on heat transfer enhancement of a ferrofluid in a closed loop oscillating heat pipe under magnetic field, Exp. Therm. Fluid Sci. 74 (2016) 265–270.
[36] H.R. Goshayeshi, M.R. Safaei, M. Goodarzi, M. Dahari, Particle size and type effects on heat transfer enhancement of Ferro-nanofluids in a pulsating heat pipe, Powder Technol. 301 (2016) 1218–1226.
[37] R. Gehr, Z.A. Zhai, J.A. Finch, S.R. Rao, Reduction of soluble mineral concentrations in $CaSO_4$ saturated water using a magnetic field, Water Res. 29 (1995) 933–940.
[38] M. Gholizadeh, H. Arabshahi, The effect of magnetic water on strength parameters of concrete, J. Eng. Technol. Res. 3 (2011) 77–81.
[39] Z. Eshaghi, M. Gholizadeh, The effect of magnetic field on the stability of (18-crown-6) complexes with potassium ion, Talanta 64 (2004) 558–561.
[40] P. Xiao-Feng, D. Bo, Investigation of changes in properties of water under the action of a magnetic field, Sci. China, Ser. G 51 (2008) 1621–1632.
[41] E.J.L. Toledo, T.C. Ramalho, Z.M. Magriotis, Influence of magnetic field on physical–chemical properties of the liquid water: insights from experimental and theoretical models, J. Mol. Struct. 888 (2008) 409–415.
[42] M.C. Amiri, A. Dadkhah, On reduction in the surface tension of water due to magnetic treatment, Colloids Surf., A 278 (2006) 252–255.
[43] P. Xiao-Feng, D. Bo, The changes of macroscopic features and microscopic structures of water under influence of magnetic field, Physica B 403 (2008) 3571–3577.
[44] Y. Cho, S. Lee, Reduction in the surface tension of water due to physical water treatment for fouling control in heat exchangers, Int. Commun. Heat Mass Transfer 32 (2005) 1–9.
[45] T. Rohani Bastami, M.H. Entezari, Synthesis of manganese oxide nanocrystal by ultrasonic bath: effect of external magnetic field, Ultrason. Sonochem. 19 (2012) 830–840.
[46] F. Moosavi, M. Gholizadeh, Magnetic effects on the solvent properties investigated by molecular dynamics simulation, J. Magn. Magn. Mater. 354 (2014) 239–247.
[47] M. Gholizadeh, G.H. Rounaghi, I. Razavipanah, M.R. Salavati, Effect of magnetic field on property of a non-aqueous solvent upon complex formation between kryptofix 22DD with yttrium (III) cation, J. Iran. Chem. Soc. 11 (2014) 947–952.
[48] B. Bazubandi, E. Moaseri, M. Baniadam, M. Maghrebi, M. Gholizadeh, Fabrication of multi-walled carbon nanotube thin films via electrophoretic deposition process: effect of water magnetization on deposition efficiency, Appl. Phys. A 120 (2015) 495–502.
[49] A. Nakhaei Pour, J. Karimi, S. Taghipoor, M. Gholizadeh, M. Hashemian, Fischer-Tropsch synthesis over CNT-supported cobalt catalyst: effect of magnetic field, J. Iran. Chem. Soc. 14 (2017) 1477–1488.
[50] H. Rashidi, A. Ahmadpour, F.F. Bamoharram, M.M. Heravi, A. Ayati, The novel, one step and facile synthesis of ZnO nanoparticles using heteropolyoxometalates and their photoluminescence behavior, Adv. Powder Technol. 24 (2013) 549–553.
[51] F.F. Bamoharram, Preparation of ZnO nanorods in the presence of nano preyssler as agreen and eco-friendly polyoxometalate and its photocatalytic activity in the photodegradation of methyl orange, Synth. React. Inorg., Met.-Org., Nano-Met. Chem. 41 (2011) 571–576.
[52] H. Rashidi, A. Ahmadpour, F. Bamoharram, S. Zebarjad, M. Heravi, F. Tayari, Controllable one-step synthesis of ZnO nanostructures using molybdophosphoric acid, Chem. Pap. 68 (2014) 516–524.
[53] E. Esmaeilnezhad, H.J. Choi, M. Schaffie, M. Gholizadeh, M. Ranjbar, Characteristics and applications of magnetized water as a green technology, J. Cleaner Prod. 161 (2017) 908–921.
[54] S.-N. Sayyed Jalal, G. Mostafa, A. Ali, R.-C. Faramarz, ZnO-nanorods as an efficient heterogeneous catalyst for the synthesis of thiazole derivatives in water, Comb. Chem. High Throughput Screen. 20 (2017) 304–309.
[55] K.-T. Chang, C.-I. Weng, The effect of an external magnetic field on the structure of liquid water using molecular dynamics simulation, J. Appl. Phys. 100 (2006) 043917.
[56] H. Hosoda, H. Mori, N. Sogoshi, A. Nagasawa, S. Nakabayashi, Refractive indices of water and aqueous electrolyte solutions under high magnetic fields, J. Phys. Chem. A 108 (2004) 1461–1464.
[57] M. Iwasaka, S. Ueno, Structure of water molecules under 14 T magnetic field, J. Appl. Phys. 83 (1998) 6459–6461.
[58] A.D. Becke, Density-functional thermochemistry. III. The role of exact exchange, J. Chem. Phys. 98 (1993) 5648–5652.

[59] C. Lee, W. Yang, R.G. Parr, Development of the Colle-Salvetti correlation-energy formula into a functional of the electron density, Phys. Rev. B 37 (1988) 785–789.
[60] M.J. Frisch, G.W. Trucks, H.B. Schlegel, G.E. Scuseria, M.A. Robb, J.R. Cheeseman, J.A. Montgomery, Jr., T. Vreven, K.N. Kudin, J.C. Burant, J.M. Millam, S.S. Iyengar, J. Tomasi, V. Barone, B. Mennucci, M. Cossi, G. Scalmani, N. Rega, G.A. Petersson, H. Nakatsuji, M. Hada, M. Ehara, K. Toyota, R. Fukuda, J. Hasegawa, M. Ishida, T. Nakajima, Y. Honda, O. Kitao, H. Nakai, M. Klene, X. Li, J.E. Knox, H. P. Hratchian, J.B. Cross, V. Bakken, C. Adamo, J. Jaramillo, R. Gomperts, R.E. Stratmann, O. Yazyev, A.J. Austin, R. Cammi, C. Pomelli, J.W. Ochterski, P.Y. Ayala, K. Morokuma, G.A. Voth, P. Salvador, J.J. Dannenberg, V.G. Zakrzewski, S. Dapprich, A.D. Daniels, M.C. Strain, O. Farkas, D.K. Malick, A.D. Rabuck, K. Raghavachari, J.B. Foresman, J.V. Ortiz, Q. Cui, A.G. Baboul, S. Clifford, J. Cioslowski, B.B. Stefanov, G. Liu, A. Liashenko, P. Piskorz, I. Komaromi, R.L. Martin, D.J. Fox, T. Keith, M.A. Al-Laham, C.Y. Peng, A. Nanayakkara, M. Challacombe, P.M. W. Gill, B. Johnson, W. Chen, M.W. Wong, C. Gonzalez, J.A. Pople, Gaussian 03, Revision C.02, Gaussian, Inc., Wallingford CT, 2004.
[61] J.S. Murray, K. Sen, Molecular Electrostatic Potentials: Concepts and Applications, first ed., Elsevier, 1996.
[62] C.M. Breneman, K.B. Wiberg, Determining atom-centered monopoles from molecular electrostatic potentials. The need for high sampling density in formamide conformational analysis, J. Comput. Chem. 11 (1990) 361–373.
[63] F. Weinhold, C.R. Landis, Natural bond orbitals and extensions of localized bonding concepts, Chem. Educ. Res. Pract. 2 (2001) 91–104.
[64] E.D. Glendening, C.R. Landis, F. Weinhold, Natural bond orbital methods, Wiley Interdiscipl. Rev.: Comput. Mol. Sci. 2 (2012) 1–42.
[65] G. García-Miaja, J. Troncoso, L. Romaní, Excess properties for binary systems ionic liquid + ethanol: experimental results and theoretical description using the ERAS model, Fluid Phase Equilib. 274 (2008) 59–67.
[66] C.L. Yaws, R.W. Pike, Density of liquid-Organic compounds, in: Thermophysical Properties of Chemicals and Hydrocarbons, William Andrew Publishing, Norwich, NY, 2009, pp. 106–197.
[67] C.I. Benmore, Y.L. Loh, The structure of liquid ethanol: a neutron diffraction and molecular dynamics study, J. Chem. Phys., 112 (2000) 5877-5883.
[68] W.L. Jorgensen, D.S. Maxwell, J. Tirado-Rives, Development and testing of the OPLS all-atom force field on conformational energetics and properties of organic liquids, J. Am. Chem. Soc. 118 (1996) 11225–11236.
[69] W.D. Cornell, P. Cieplak, C.I. Bayly, I.R. Gould, K.M. Merz, D.M. Ferguson, D.C. Spellmeyer, T. Fox, J.W. Caldwell, P.A. Kollman, A second generation force field for the simulation of proteins, nucleic acids, and organic molecules, J. Am. Chem. Soc. 117 (1995) 5179–5197.
[70] S.L. Mayo, B.D. Olafson, W.A. Goddard, DREIDING: a generic force field for molecular simulations, J. Phys. Chem. 94 (1990) 8897–8909.
[71] L. Saiz, J. Padro, E. Guardia, Structure and dynamics of liquid ethanol, J. Phys. Chem. B 101 (1997) 78–86.
[72] M. Kohagen, M. Brehm, J. Thar, W. Zhao, F. Müller-Plathe, B. Kirchner, Performance of quantum chemically derived charges and persistence of ion cages in ionic liquids. A molecular dynamics simulations study of 1-n-butyl-3-methylimidazolium bromide, J. Phys. Chem. B 115 (2010) 693–702.
[73] O. Guvench, S.N. Greene, G. Kamath, J.W. Brady, R.M. Venable, R.W. Pastor, A.D. Mackerell, Additive empirical force field for hexopyranose monosaccharides, J. Comput. Chem. 29 (2008) 2543–2564.
[74] L. Weng, C. Chen, J. Zuo, W. Li, Molecular dynamics study of effects of temperature and concentration on hydrogen-bond abilities of ethylene glycol and glycerol: implications for cryopreservation, J. Phys. Chem. A 115 (2011) 4729–4737.
[75] C. Chen, W.Z. Li, Y.C. Song, J. Yang, Hydrogen bonding analysis of glycerol aqueous solutions: a molecular dynamics simulation study, J. Mol. Liq. 146 (2009) 23–28.
[76] M.P. Allen, D.J. Tildesley, Computer Simulation of Liquids, Oxford Science Publications, 1989.
[77] S. Melchionna, G. Ciccotti, B. Lee Holian, Hoover NPT dynamics for systems varying in shape and size, Mol. Phys. 78 (1993) 533–544.
[78] W. Smith, T.R. Forester, DL_POLY_2.0: A general-purpose parallel molecular dynamics simulation package, J. Mol. Graph. 14 (1996) 136–141.
[79] Q. Li, E. Wang, S. Li, C. Wang, C. Tian, G. Sun, J. Gu, R. Xu, Template-free polyoxometalate-assisted synthesis for ZnO hollow spheres, J. Solid State Chem. 182 (2009) 1149–1155.
[80] J.M.D. Coey, S. Cass, Magnetic water treatment, J. Magn. Magn. Mater. 209 (2000) 71–74.
[81] H.E.L. Madsen, Influence of magnetic field on the precipitation of some inorganic salts, J. Cryst. Growth 152 (1995) 94–100.
[82] Z. Wang, X.F. Qian, J. Yin, Z.K. Zhu, Large-scale fabrication of tower-like, flower-like, and tube-like ZnO arrays by a simple chemical solution route, Langmuir 20 (2004) 3441–3448.
[83] J. Zhang, L. Sun, J. Yin, H. Su, C. Liao, C. Yan, Control of ZnO morphology via a simple solution route, Chem. Mater. 14 (2002) 4172–4177.
[84] R. Cai, H. Yang, J. He, W. Zhu, The effects of magnetic fields on water molecular hydrogen bonds, J. Mol. Struct. 938 (2009) 15–19.
[85] Z.A. Peng, X. Peng, Mechanisms of the shape evolution of CdSe nanocrystals, J. Am. Chem. Soc. 123 (2001) 1389–1395.
[86] Z.A. Peng, X. Peng, Nearly monodisperse and shape-controlled CdSe nanocrystals via alternative routes: nucleation and growth, J. Am. Chem. Soc. 124 (2002) 3343–3353.
[87] I. Benjamin, Theoretical study of the water/1,2-dichloroethane interface: structure, dynamics, and conformational equilibria at the liquid–liquid interface, J. Chem. Phys. 97 (1992) 1432–1445.
[88] M. Levitt, M. Hirshberg, R. Sharon, K.E. Laidig, V. Daggett, Calibration and testing of a water model for simulation of the molecular dynamics of proteins and nucleic acids in solution, J. Phys. Chem. B 101 (1997) 5051–5061.